Thin-Walled Structures 96 (2015) 56–63

Contents lists available at ScienceDirect

Thin-Walled Structures

journal homepage: www.elsevier.com/locate/tws

External pressure induced buckling collapse of high density polyethylene (HDPE) liners: FEM modeling and predictions

F. Rueda [a,*], J.P. Torres [a], M. Machado [b], P.M. Frontini [a], J.L. Otegui [a]

[a] Instituto de Tecnología y Ciencia de Materiales, Universidad Nacional de Mar del Plata, B7608FDQ Argentina
[b] Johannes Kepler University Linz, Institute of Polymer Product Engineering, Altenbergerstrasse 69, 4040 Linz, Austria

ARTICLE INFO

Article history:
Received 4 December 2013
Received in revised form
5 March 2015
Accepted 27 April 2015

Keywords:
Buckling collapse
Constitutive modeling
HDPE liners
Finite element modeling

ABSTRACT

Thermoplastic polymers such as HDPE are nowadays widely used as lining materials for oil and gas pipelines. However, during maintenance or unexpected service stoppages, these liners can undergo external pressure induced bucking collapse. The objective of this work is to assess the mechanical response of HDPE liners undergoing buckling collapse by means of Finite element modeling (FEM) simulations on Abaqus 6.10. To accomplish this, an advanced constitutive model, namely the Three Network Model (TNM) was employed. In order to determine the input parameters for the model, a series of tensile and compressive uniaxial tests were conducted. The suitability of the model for this particular application was assessed by contrasting the simulation and the experimental results of a diametral compression test. The complex strain rate and pressure dependent mechanical response of HDPE liners was analyzed by modeling the buckling collapse dynamic event as an increasing volume of fluid entering the gap cavity between liner and host pipe. The model predictions allowed establishing a mathematical relationship between the depressurization velocity of the tubes and the resulting collapse pressure. These relations can be used to improve the current design guidelines for plastic liners.

1. Introduction

Nowadays the use of polymers in the gas and oil transportation industry is widely spread. One of their main uses is as lining materials for oil and gas pipelines. These liners serve the function of providing internal protection of metallic tubes mainly in two different situations; namely in providing enhanced corrosion resistance from aggressive chemical agents, and, in rehabilitating/lining damaged pipelines. During these situations, pipelines are slip lined with a polyethylene liner that replaces the inoperative section of the tube [1]. However, there is a number of ways in which polymeric liners can fail in service after a certain time. The present study is specifically concerned with the buckling collapse of liners induced by external pressure. This failure mode takes place by the combined action of two separate factors: (i) the permeation of oil derived gases through the liner wall for extended periods of time, and (ii) the rapid decompression of pipelines that can occur during service stoppages or maintenance and inspection shutdowns [2].

A number of studies have been devoted to understand the underlying mechanisms that eventually lead to liner failure [3–6]. Material failure is associated with the phenomenon known as physical swelling [7,8]. This occurs when some organic components, such as the CO_2 and CH_4 dissolved in oil, penetrate into the polymer macromolecular chain network of the liner aided by the high pressure operating conditions, increasing the space between molecules and decreasing the intermolecular bonding. As this operation takes place, the migratory gases can permeate throughout the liner wall and gradually balance the pressure difference between the inside of the liner and the annular region consisting of the gap between the liner and the pipe wall. This permeation mechanism worsens recursively since permeation rate increases with the severity of swelling of the liner. Finally, buckling collapse occurs when the liner is intentionally decompressed and the external pressure built up by the confined gases in the annular region, generates a stress state in the liner that induces the radial buckling failure.

On the other hand, a number of analytical models that deal with the buckling collapse of metallic tubes under external pressure have been developed in the literature [9–11]. In [9], Glock derived a model, based on the principle of minimal potential energy and non-linear deformation theory, which allowed for the determination of the critical pressure for the buckling collapse of a restrained tube under external pressure. It must be noted that Glock's model does not account for plastic deformation and therefore it is mainly restricted to thin walled pipes that fail by

* Corresponding author.
E-mail address: federico.rueda@fi.mdp.edu.ar (F. Rueda).

http://dx.doi.org/10.1016/j.tws.2015.04.035
0263-8231/

elastic buckling before yielding. Conversely, in [10] Jacobsen developed a semi-analytical model which predicts the critical pressure at which a tube experiences yielding at some location. This critical pressure value can be used as a conservative design value for the design of thick pipes, for which yielding occurs before reaching the buckling pressure. Following this, in [11] El-Sawy defined two different collapse regimes: (i) elastic buckling collapse, where buckling failure occurs before the pipe reaches the material yield stress at any point; and (ii) inelastic buckling collapse, which occurs after the onset of plastic deformation and, therefore, at a higher pressure than the critical pressure for reaching material yield stress. While considering that low thickness-to-diameter (w/D) aspect ratios and high yield-to-stiffness (σ_y/E') ratios tend to favor elastic collapse, and that high w/D ratios and low σ_y/E' ratios favor inelastic collapse, El-Sawy proposed a relationship that allows for the identification of collapse regime as a function of these ratios for an ideal elastoplastic material:

$$\frac{\sigma_y}{E'} = 1.45\left(\frac{w}{D}\right) + 3.93\left(\frac{w}{D}\right)^2 \quad (1)$$

where w is the pipe wall thickness, D is the pipe diameter, σ_y is the yield stress, $E'=E/(1-\nu^2)$, E is the elastic modulus and ν is Poisson's ratio. The resulting w/D vs. σ_y/E' curve denotes the limit between elastic and inelastic collapse. It is important to remark that these analytical solutions are restricted to purely elastic or ideal elastoplastic behavior and are then insufficient to describe the behavior of time-dependent materials such as thermoplastic polymers, for which the relationship σ_y/E' is highly strain-rate dependent and therefore different for every point along the pipe's cross-section.

Nevertheless, these analytical models [9,10] cannot analyze the influence of geometrical or surface defects, so commonly generated during the manufacturing, storage, transport and installation stages, and are only useful for obtaining a critical pressure value and are not able to describe the whole deformation process. To overcome these limitations, Rueda et al. [12] were able to develop the FEM model for the simulation of the buckling collapse of HDPE liners. In their work, they successfully simulated an overall buckling collapse situation by introducing hydrostatic fluid elements in the model to allow for hydraulic effects. For the description of material constitutive response, they analyzed 3 different types of material behavior: linear elastic and linear elastoplastic with and without strain hardening. Their investigation served as the first step for the prediction of actual failure situations since it showed that the collapse event could be effectively simulated by FEM analysis in order to account for time-dependent effects. Unfortunately, the traditional constitutive models used in all previous investigations cannot account for the intrinsic strain-rate, pressure and temperature dependence of polymer mechanical behavior and therefore are not adequate to reproduce the complex multiaxial stress response and rate-dependent deformation evolution that will take place during an actual rapid pipe depressurization situation. As a consequence, it remains to include into the analysis an advanced constitutive model capable of accounting for the intricate response of polymers.

Constitutive modeling of polymers is currently a well-established field with a large number of advances over the last 40 years. In this regard, one of the most successful developments has been the family of tridimensional constitutive models started by Boyce and coworkers [13–17], which brought together current theories of macromolecular physics with recent work in the fields of statistical mechanics, continuum mechanics, and computational mechanics. These models employ a constitutive framework intended to be general enough to capture material behavior over a wide range of loading conditions, in order to be appropriate for their use in FEM analysis. The original work of Boyce et al. [13] was concerned with the large viscoplastic deformation of amorphous polymers, such as polycarbonate (PC) and acrylic glass (PMMA). So far, this constitutive approach has been consecutively enhanced in order to include additional features of polymer deformation such as, strain induced anisotropy, rubber elasticity, thermo-mechanical coupling, high strain-rate testing and so on. Among these, a notable contribution was the Hybrid Model (HM) of Bergstrom et al. [18] which was designed for capturing the mechanical response of a semi-crystalline polymer: Ultra-high molecular weight polyethylene (UHMWPE). Following this, in [19], Bergstrom et al. developed the Three Network Model (TNM) which is a further refinement of the HM model to be more accurate and computationally efficient. For its pertinence regarding semi-crystalline thermoplastic polymers, the TNM model results in a suitable choice for modeling the mechanical response of HDPE liners. In the present work, the evaluation and validation of the TNM model, for its use in the FEM to accurately predict the buckling failure in pipes in a varying range of temperature and loading-rate conditions, is performed.

2. Experimental

2.1. Uniaxial tensile and compression tests

For the calibration of the TNM material model, tensile and compression tests were performed on an Instron 4467 universal testing machine. Tensile and compression specimens were machined out from a supplied liner. A total of nine specimens for each loading case were used. In order to univocally determine the viscous parameters, the tests were carried out at 3 different strain-rates, corresponding to cross head speeds of 1, 10 and 50 mm/min. Tensile tests were performed using an extensometer of 12.5 mm gauge length on 2.5 mm × 2.5 mm cross-section dogbone-shaped specimens (the remaining specimen dimensions correspond to the type V^C specimens described in the ASTM D638-03 standard test method [20]). Compression tests were carried out employing specimens of approximately 10 mm in height and 5 mm in diameter according to 2:1 (height:diameter) ratio recommended in [21]. For a complete characterization of deformation evolution, both loading and unloading response was registered. The analytic procedure for parameter determination from uniaxial tests results is explained later in Section 3.1.

2.2. Diametral compression test

Once the TNM constitutive model was calibrated using uniaxial test results (see Section 3.1), the following logical step was to validate the model predictions for a stress state that is closer to the actual service conditions. To this aim, diametral compression tests were carried out using the 3-point flexure test fixture (Fig. 1a). 57 mm ring-shaped specimens were cut from the liner and loaded at 50, 100 and 500 mm/min crosshead speeds.

3. Computational efforts

3.1. Constitutive model

The main aspects of the TNM model constitutive framework will be described below, more details on the formulation can be found in the original works [18–19]. The TNM model consists of three networks acting in parallel. A simplified unidimensional rheological representation can be seen in Fig. 2.

Networks A and B represent the initial viscoplastic response, which is captured using two separate energy activation deformation mechanisms corresponding to amorphous and semicrystalline

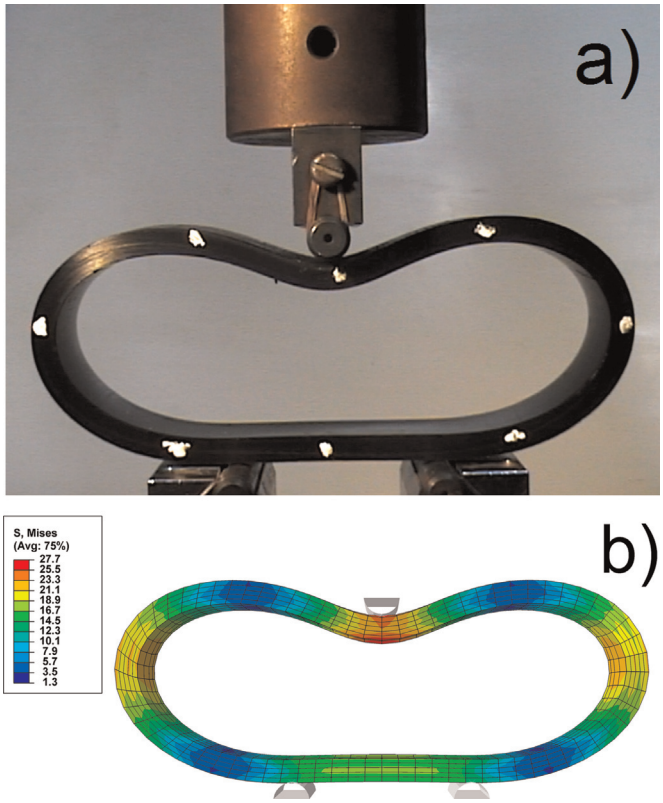

Fig. 1. Diametral compression test for the liner ring section. (a) Experimental setup. (b) FEM simulation. (All stresses in MPa).

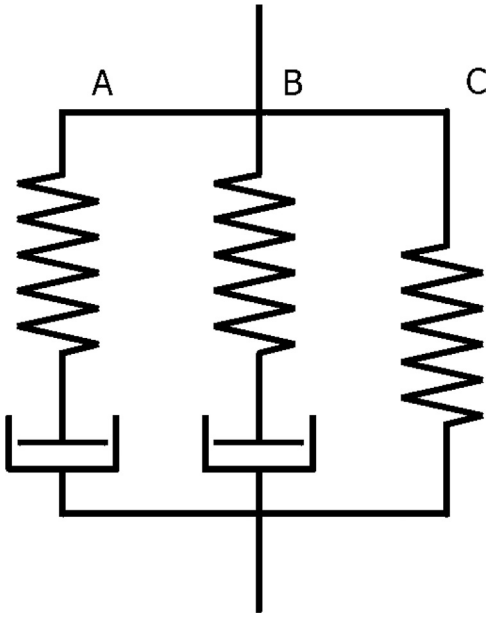

Fig. 2. Rheological unidimensional representation of the TNM constitutive model.

domains of the polymer. Network C captures the overall non-viscous hyperelastic component of the material response, i.e. the entropic chain stretch hardening. The total deformation gradient (F^{app}) of the assembly is decomposed into a thermal expansion component (F^{th}) and a mechanical deformation component (F):

$$\mathbf{F}^{app} = \mathbf{F}\mathbf{F}^{th} \tag{2}$$

The mechanical deformation gradient of networks A and B are further decomposed into elastic and viscoplastic components:

$$\mathbf{F} = \mathbf{F}_n^e\mathbf{F}_n^v \tag{3}$$

where n takes the value A and B, for networks A and B correspondingly. $\mathbf{F}_n^e$ is the elastic component of thedeformation gradient, which is constitutively determined from Eq. (4). $\mathbf{F}_n^v$is the viscoplastic component of $\mathbf{F}$and is constitutively determined from Eqs. ((6) and 7).

The Cauchy stress acting in networks A and B has the following form:

$$\boldsymbol{\sigma}_n = \frac{\mu_n}{J_n^e\overline{\lambda_n^{e*}}}[1 + \frac{\theta-\theta_0}{\hat{\theta}}]\frac{\mathbf{L}^{-1}(\overline{\lambda_n^{e*}}/\lambda_L)}{\mathbf{L}^{-1}(1/\lambda_L)}\mathrm{dev}[\mathbf{b}_n^{e*}] + \kappa(J_n^e - 1)\mathbf{1} \tag{4}$$

where, $J_n^e = \det[\mathbf{F}_n^e]$; $\mathbf{b}_n^{e*} = (J_n^e)^{-2/3}\mathbf{F}_n^e(\mathbf{F}_n^e)^{\mathrm{T}}$is the Cauchy–Green deformation tensor; θ is the current temperature; θ_0 is a reference temperature; $\hat{\theta}$ is a material parameter specifying the temperature response of stiffness; $\bar{\lambda}_n^{e*} = (\mathrm{tr}[\mathbf{b}_n^{e*}]/3)^{1/2}$is the effective chain stretch and $\mathbf{L}^{-1}(x)$is the inverse Langevin function; μ_n is the elastic shear modulus of network n and κ is the bulk modulus. These material constants can be interpreted as analogous to the linear elastic shear and bulk modulus, with the difference that in the TNM model the shear modulus is scaled by the Langevin function. λ_L is the locking stretch and gives a measure of the hyperelastic hardening response at large strains.

The velocity gradient of networks A and B have the following form:

$$\dot{\mathbf{F}}_n^v = \dot{\gamma}_n\mathbf{F}_n^{e-1}\frac{dev[\boldsymbol{\sigma}_n]}{\tau_n}\mathbf{F} \tag{5}$$

Where the flow rate $\dot{\gamma}$is given by a power-law flow equation:

$$\dot{\gamma}_n = \dot{\gamma}_0(\frac{\tau_n}{\hat{\tau}_n + aR(p_n)})^{m_n}(\frac{\theta}{\theta_0})^n \tag{6}$$

Here $\dot{\gamma}_0[\frac{1}{s}]$ is a constant introduced for dimensional consistency, $R(x)$ is the ramp function; p_n is the hydrostatic pressure; τ_n is the Fronebius norm of the deviatoric part of σ_n; τ_n is the flow resistance of network n and gives a measure of the shear stress at which plastic flow becomes a dominant deformation mechanism; m is the stress exponential of the power-law equation and mainly determines the material strain-rate sensitivity.

The Cauchy stress acting in network C has the following form:

$$\boldsymbol{\sigma}_C = \frac{1}{1+q}\{\frac{\mu_C}{J\lambda_{chain}}[1 + \frac{\theta-\theta_0}{\hat{\theta}}]\frac{\mathbf{L}^{-1}(\lambda_{chain}/\lambda_L)}{\mathbf{L}^{-1}(1/\lambda_L)}\mathrm{dev}[\mathbf{b}^*] + \kappa(J-1)\mathbf{1} + q\frac{\mu_C}{J}[I_1^*\mathbf{b}^* - \frac{2I_2^*}{3}\mathbf{I} - (\mathbf{b}^*)^2]\} \tag{7}$$

where $J = \det[\mathbf{F}]$; $\mathbf{b}^* = J^{-2/3}\mathbf{F}(\mathbf{F})^{\mathrm{T}}$is the Cauchy–Green deformation tensor, and $\lambda_{chain} = (\mathrm{tr}[\mathbf{b}^*]/3)^{1/2}$.

Finally, since they are in parallel, the three networks have equal mechanical deformation gradients and the total stress of the system is the sum of each network stress. The TNM model was executed as a user material subroutine (UMAT/VUMAT) for ABAQUS using the PolyUmod material libraries [22].

The constitutive parameters for all presented constitutive models were determined using a parameter-extraction software, namely MCalibration [23], which enables semi-automatic extraction of material parameters using as input different loading cases (monotonic, dynamic mechanical anaylisis, creep, etc.) with several loading modes (uniaxial, biaxial, plane stress, etc.) for a variety of advanced constitutive models, including elastoplastic behavior

and the TNM model. This software determines parameter values using a minimization algorithm based on the Nelder-Mead simplex method [24]. This method uses iterations to evaluate the difference between the model predictions and the experimental results in a least-squares sense, i.e. using a minimum squares cost function. In each iteration, the method tries new estimations for the constitutive parameters using an approximation criterion and the iterations continue until the cost function reaches an established minimum. Initial values and upper and lower bound values for the optimization method are already predefined in the calibration software using typical thermoplastic material constitutive parameters [19].

3.2. Diametral compression FEM model

The diametral compression test was simulated in ABAQUS/Standard 6.10 using both the TNM model and the traditional elastoplastic model (Von Mises yielding surface with isotropic hardening [25]). Both models were calibrated using the uniaxial test data and were then contrasted with the experimental results. For the comparison to be consistent, the traditional elastoplastic stress–strain relationship was also calibrated using 3 different strain–rates and a least-squares minimization algorithm using MCalibration (see previous section). Since the elastoplastic model is strain–rate independent, this means that the material parameters found are those that produce the smaller difference between the models' prediction and the experimental results for all 3 stress–strain relationships, simultaneously.

This approach allows comparing the prediction capability of the TNM model and its superiority, against the commonly used plasticity model, in modeling the strain–rate dependency and also the pressure dependency (i.e. the influence of the hydrostatic stress, $\sigma_{Hyd} = (\sigma_{11} + \sigma_{22} + \sigma_{33})/3$, on resistance to plastic flow) of polymer behavior. The supports and loading tip were modeled as rigid solids. A total of 1640 C3D8H (8-node linear brick) elements were used to model the liner ring (Fig. 1b). Frictionless tangential and rigid normal contact conditions (termed as "hard contact" in Abaqus) were employed. Loading was modeled by imposing a displacement on the loading tip. Simulations were carried out for 50, 100 and 500 mm/min loading velocities.

3.3. Buckling collapse of a liner: FEM model

The buckling collapse event was simplified assuming an ideal vacuum in the interior cavity of the liner and an increasing volume of fluid entering the liner-pipe annulus cavity at a constant fluid flow rate q_{cav}. This simplification has been made since this situation is easier to reproduce experimentally under controlled laboratory conditions. The event was simulated using ABAQUS/Standard 6.10 for q_{cav}values ranging from 10^{-8} to 10^{8} cm^3/s, and thickness-to-diameter w/D values ranging from 0.03 to 0.11.

The thermoplastic liner was modeled as a planar bidimensional deformable solid using CPE8R elements and assuming plain strain conditions, i.e. neglecting the effect of restraint at the liner ends. This assumption has proven to be valid for length to radius values greater than 6 [26]. A small elliptical curvature (i.e. a 0.4% difference between the lower-half y-radius and the upper-half y-radius values) was introduced in the upper part of the liner along the y-axis in order to induce single lob buckling (Fig. 3) in this region, which is the most critical failure mode and the most frequently observed in practice. Symmetry conditions were imposed with respect to the vertical axis. The external metallic tube was assumed to be completely rigid in order to save CPU time. The fluid was modeled using F2D2 hydrostatic fluid elements and the depressurization event was modeled by imposing a fluid volume flux

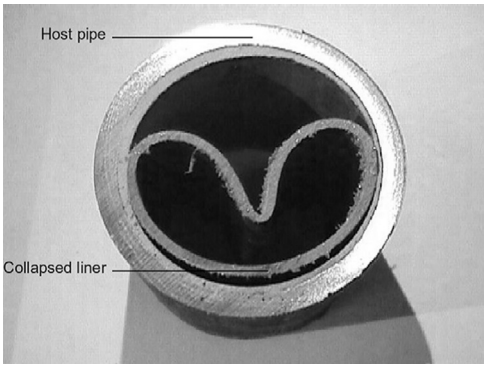

Fig. 3. Single lob failure mode geometry.

using the "fluid flux" option in ABAQUS/Standard. A classical static FEM analysis would have involved imposing a continuously increasing pressure on the outer liner surface. However, for the present analysis, this approach typically fails at the peak (i.e. buckling) pressure. In other words, pressure evolution in the cavity cannot be imposed beforehand as an independent variable. Therefore, the fluid volume flux approach is more pertinent since it models the real cause of pressure increase, i.e. the entrance of a fluid into the annulus. The previous study of the application of this method in modeling liner buckling collapse can be found in [12]. The hydrostatic fluid elements are surface elements that cover the boundary of fluid containing cavity and provide the coupling between the deformation of the fluid-filled solid and the pressure exerted by the contained fluid on the solid surface defined as cavity boundary [25].

4. Results & discussion

4.1. Uniaxial tensile and compression tests

Tensile and compression tests results at different strain rates are shown together in Fig. 4. In both cases, an initial time-independent elastic response can be observed. At a stress value between 5 and 10 MPa the material enters the visco-elastoplastic regime, this region corresponds to the complex onset of different plastic flow mechanisms in the amorphous and semicrystalline domains of the thermoplastic material [18,19]. In the constitutive model, the deformation gradients of the dashpots, which were at

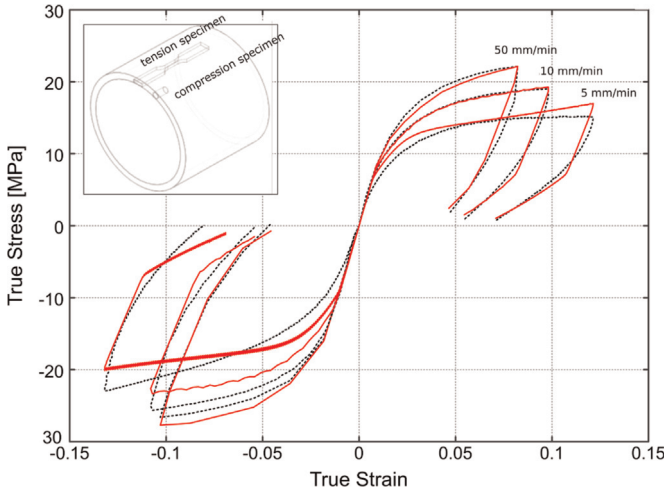

Fig. 4. Uniaxial tensile and compression results at 1, 10 and 50 mm/min cross-head speeds for HDPE. Dotted and solid lines are experimental and model prediction values respectively. The box on the upper left corner shows the tensile and compression specimens as obtained from the liner.

Table 1
Constitutive parameters for the TNM model (all values were determined at ambient temperature).

Symbol	Name	Value
μ_A	Shear modulus of network A	40 MPa
λ_L	Chain locking stretch	1.02
$\hat{\theta}$	Temperature response of stiffness	−300 K
κ	Bulk modulus	2000 MPa
$\hat{\tau}_A$	Flow resistance of network A	2.07 MPa
a	Pressure dependence of flow	0.36
m_a	Stress exponential of network A	5.15
m_b	Stress exponential of network B	22.35
n	Viscosity parameter	40
$\hat{\tau}_B$	Flow resistance of network B	16.9 MPa
μ_{Bi}	Initial shear modulus of network B	259.3 MPa
μ_{Bf}	Final shear modulus of network B	60.51 MPa
μ_C	Shear modulus of network C	≈ 0
q	Relative contribution of I_2 of network C	0

Table 2
Constitutive parameters for the elastoplasticity model (all values were determined at ambient temperature).

Young Modulus (MPa)	Poisson's ratio
496.3	0.44
Yield Stress (MPa)	**Plastic strain**
12.9	0
15.7	0.0035
17.6	0.020
26.1	0.131

first negligible, start to flow at these stress values. Also in this regime, hardening is observed with increasing the strain rate, as expected. The material shows strain rate sensitivity both in tension and compression. When increasing the crosshead speed from 1 mm/min to 50 mm/min, a ≈30% increase in the value of the maximum attained stress can be observed. Pressure dependency can be observed as the maximum stress achieved in compression is higher than in tension for equal deformation rates. For the TNM model, a very good fit was obtained between experimental and TNM model predictions, with a R^2 (Coefficient of Determination) value of 0.976. The constitutive parameters obtained both for the TNM and the elastoplastic model, are presented in Tables 1 and 2 respectively.

4.2. Diametral compression: FEM simulation

Experimental results for the diametral compression test were contrasted with FEM predictions both using the elastoplasticity with strain-hardening model and the TNM model (obtained as per Section 4.1.). Results for 50, 100 and 500 mm/min crosshead speeds are shown in Fig. 5. At all loading speeds it can be observed that that the traditional strain-rate independent elastoplastic model is not able to reproduce the initial stiffness of the system (the initial slope in the force–displacement curve), while the TNM model gives a much more accurate fit. On the other hand, the maximum load attained during the tests increases with the loading speed. This increment is caused by the material strain-rate dependency, in the sense that the required stress for the onset of plastic flow increases with strain-rate. This tendency is well-reproduced by the TNM model whereas the elastoplastic model always predicts the same maximum load regardless of the loading rate.

4.3. Buckling collapse of a liner: FEM simulations

Fig. 6 shows the liner cross-section after failure obtained from the Abaqus simulations, which presents the same buckling profile that is observed experimentally (Fig. 3). Results from FEM simulations are presented in Figs. 7–11.

The normalized area of the liner-pipe cavity, S*, is defined as follows:

$$S^* = \frac{S_{cav}}{S_o} \tag{8}$$

where S_{cav} represents the current area occupied by the annulus cavity as it is filled and S_0 is the initial cross section bounded by the internal pipe wall. The parameter S^* quantifies the deformation level of the liner cross-section. In addition, a normalized fluid flow rate q^* was defined as follows:

$$q^* = \frac{q_{cav}}{V_0} = \frac{V_{cav}}{V_0}.\frac{1}{t} = \frac{S_{cav}.L}{S_0.L}.\frac{1}{t} = \frac{S^*}{t}[\frac{1}{s}] \tag{9}$$

where q_{cav} is the volumetric fluid flow rate in the annulus as defined in Section 3.3,V_0 is the constant volume bounded by the host pipe, V_{cav} is the instantaneous lobe volume and L is the pipe length. The parameter q^* gives a geometrically independent measure of the velocity at which the tube is deforming. Fig. 7 shows the fluid pressure evolution as a function of S^* for several q^* values and $w/D=0.054$. The initial slopes of the P vs. S^* curves are similiar for all q^* values, this behavior is related to the initial elastic response of the material which showed negligible strain-rate dependency as was noted in the tensile test results (Fig. 4). However, it can be seen that approximately for $S^* \geq 0.005$, higher q^* values lead to a more rapid increase in fluid pressure with fluid volume. This means that, when the cavity is filled more rapidly, plastic deformation mechanisms in the polymeric liner are more difficult to activate and therefore require a higher external pressure.Fig. 8 shows the maximum pressure attained, i.e. the collapse pressure, as a function of q^*, where three clearly distinct regions can be recognized. From q^* values up to approximately 10^{-2}, an exponential relationship between collapse pressure (P_c) and q^* can be determined:

$$P_c = P_0(q^*)^R \tag{10}$$

where $P_c$is the collapse pressure, and R is a flow rate sensitivity exponent which is also expected to depend on the pipe cross section dimensions. Due to its rate-dependency, this region can be associated with the inelastic buckling collapse regime. By increasing q^*, a transition region is seen where a critical value q^*_{cr} can be determined, above which the collapse pressure becomes rate-independent. This change in behavior corresponds to the inelastic–elastic transition in collapse regime. Elastic regime is promoted at high q^* values and is characterized by independence of collapse pressure with deformation rate. Since the curves are plotted in a logarithmic scale, the slope represents the magnitude of the exponent R and the intercept represents the value of P_0.

Following this, to study the influence of geometry on collapse pressure, simulations were carried out for a range of thickness-to-diameter aspect ratios w/D. Fig. 9 presents P_{cr} vs q^* curves for the selected w/D ratios. In the inelastic region shown in Fig. 9, it can be observed that for every curve the slope changes with w/D. Similarly, the value of the pre-exponential term P_0 also depends on w/D. The dependence of R with thickness-to-diameter ratio w/D can be determined by plotting the magnitude of the slope for every w/D value. As can be seen in Fig. 10, this relationship can be approximated as linear dependent:

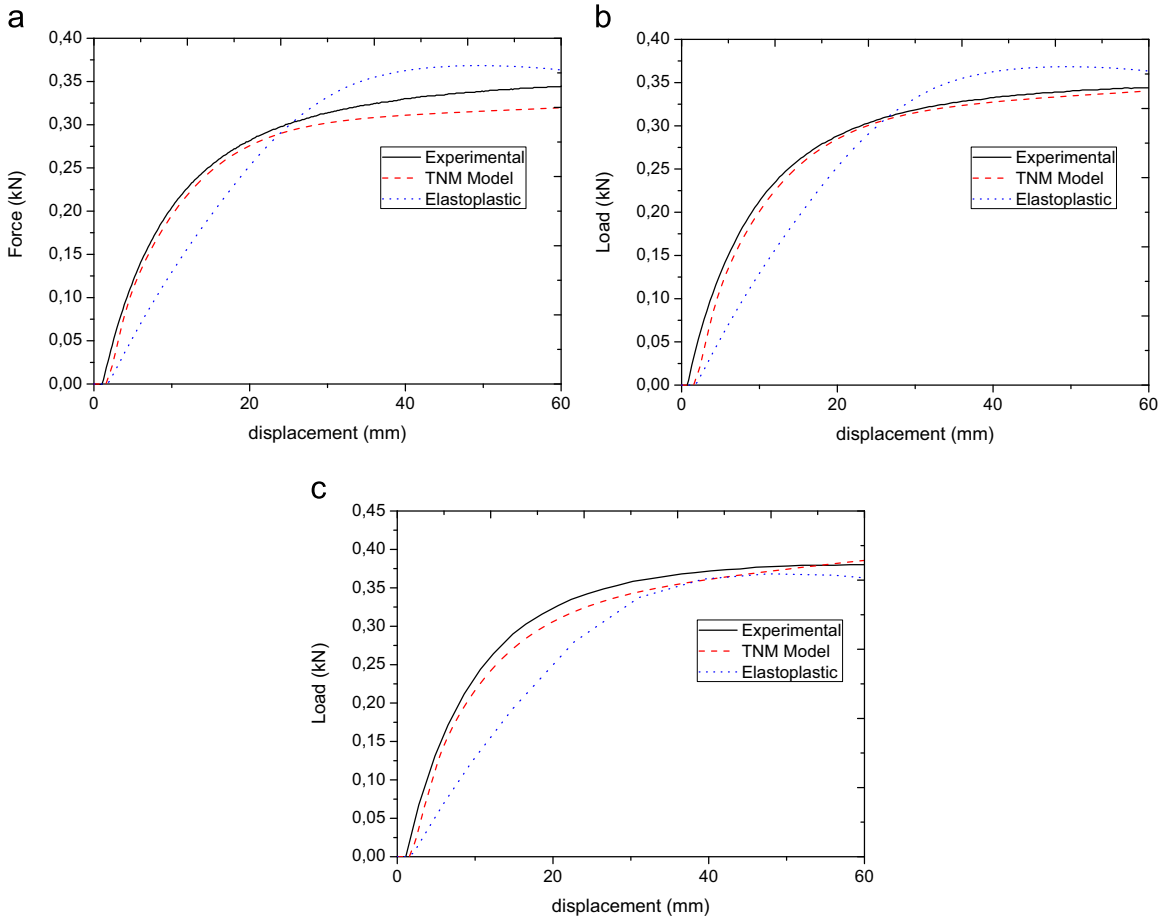

Fig. 5. Diametral compression experimental and FEM results at different loading speeds. (a) 50 mm/min, (b) 100 mm/min and (c) 500 mm/min.

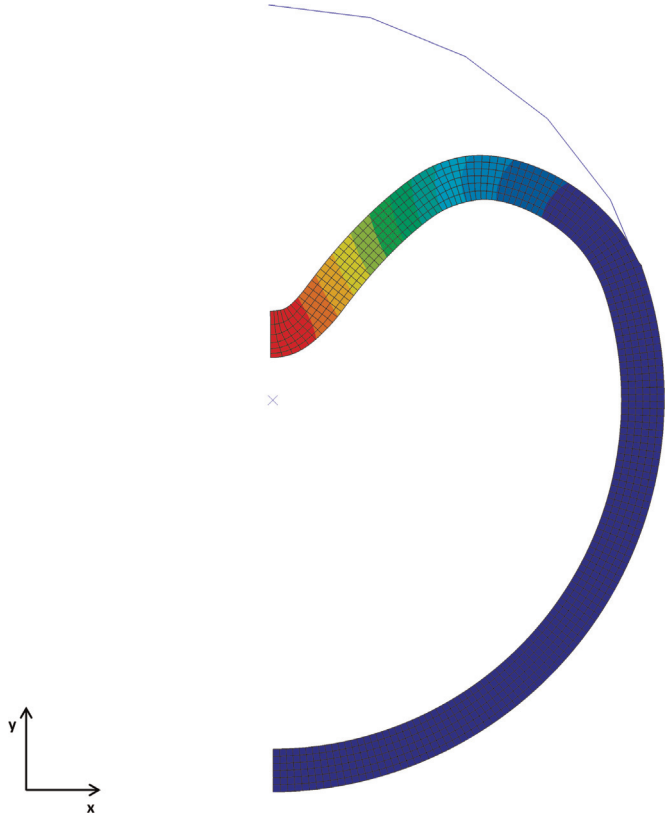

Fig. 6. Liner cross-section finite element mesh after buckling failure.

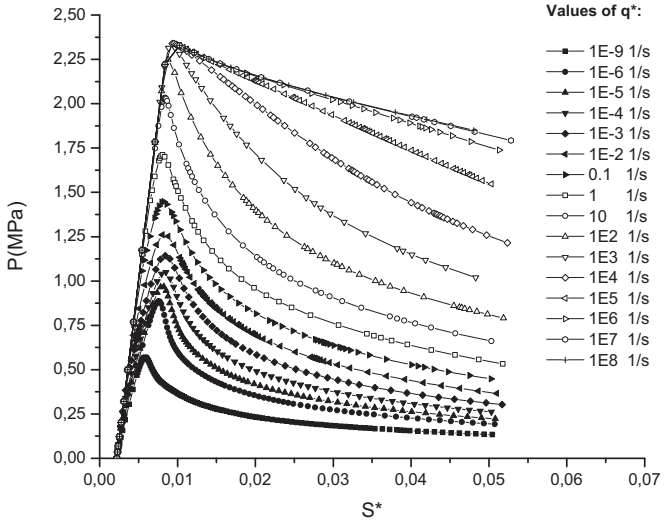

Fig. 7. Evolution of fluid pressure as a function of S^* at a wide range of normalized fluid flow rates q^* and w/D=0.054.

$$R = C_1\left(\frac{w}{D}\right) + C_2 \tag{11}$$

where R is a flow rate sensitivity parameter which characterizes the effect of material strain rate dependency on collapse pressure. If the values of in-service depressurization velocities are known, this factor can be of significant importance for the materials selection process. In addition, as can be seen in Fig. 11, the pre-

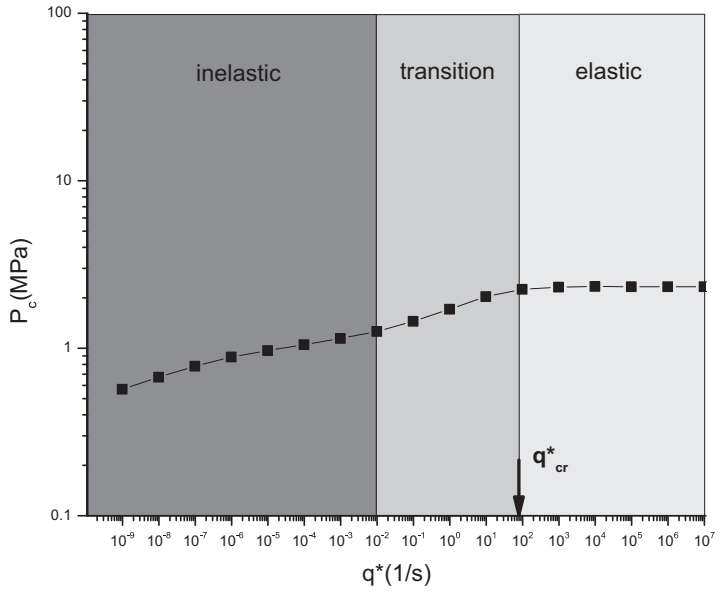

Fig. 8. Collapse pressure and failure regimes as a function of imposed fluid flow rate q^*, for $w/D = 0.054$.

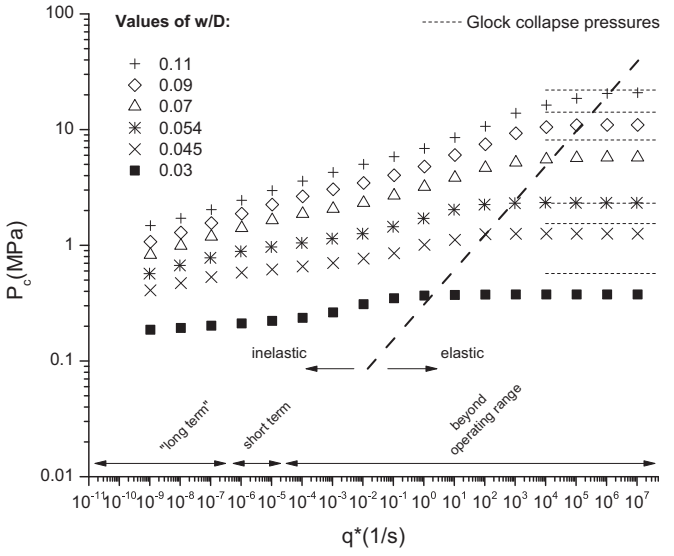

Fig. 9. Effect of parameter q* on the collapse pressure P_c at different w/D radios. Glock pressures are also shown for comparison. Elastic parameters used for Glock pressure calculations where evaluated at each strain rate from the linear range of the stress strain curves for the low strain range regime and taken from [29] at high strain rate regime.

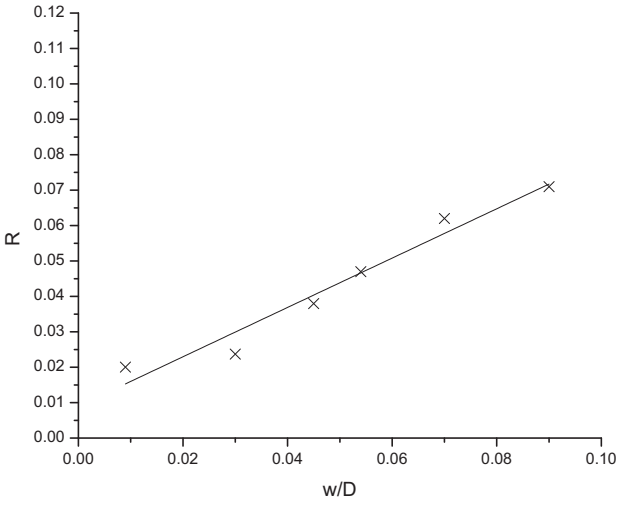

Fig. 10. Effect of w/D on the parameter R.

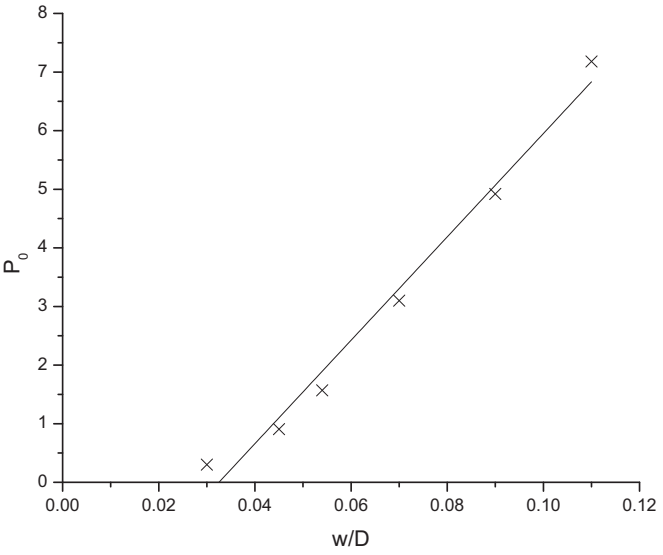

Fig. 11. Effect of w/D on the parameter P_0.

exponential term exhibits linear-dependency with w/D:

$$P_0 = C_3\left(\frac{w}{D}\right) + C_4 \tag{12}$$

For the studied HDPE, the values for the constants C_1, C_2, C_3 and $C_4$are depicted in Table 3. On the other hand, Fig. 9 also reveals that the location of inelastic-elastic transition, i.e. the q^*_{cr}value, also depends on w/D. In addition, in Fig. 9 the different ranges of technologically relevant q^* values (as considered by [27]) are shown. It can be seen here that, for the HDPE used in this investigation, all practically achievable q^* values and commonly used w/D values will show inelastic failure mode.

Eqs. (10), (11) and (12) are helpful in giving an understanding of how does polymer strain-rate dependency affects a liner response in service conditions. It is important to note that the strain-rate and temperature dependence in polymers can be correlated using

Table 3
Constants C_1, C_2, C_3, and C_4 of the HDPE liner (all values were determined at ambient temperature).

Symbol	Value
C_1	0.7
C_2	0.0054
C_3	88.19 $MPa(s^{1/R})$
C_4	-2.86 $MPa(s^{1/R})$

the time–temperature superposition (TTS) principle [28]. Therefore, the analysis presented in this investigation can be used to understand qualitatively how temperature will affect the liner response, in the sense that increasing the strain-rate has a similar effect as decreasing the temperature. However, a detailed analysis of temperature influence will be the focus of a future investigation.

5. Conclusion and forthcoming work

The external pressure-induced buckling collapse of HDPE liners was successfully simulated using the FEM while taking into account the intrinsic non-linear, time-pressure-dependent response exhibited by thermoplastic polymers. The stress-strain response of the considered HDPE material was modeled using the advanced TNM viscoelastic–viscoplastic model. Constitutive parameters were determined from tensile and compression stress–strain curves at different strain rates. The suitability of the obtained parameter of the TNM model for this particular problem was validated by running FEM simulations of the ring compression tests and comparing the results against the experimental data. The buckling failure event was predicted by performing FEM simulations for a wide range of fluid flow rates q^*. It was found that the material strain rate dependency has a significant effect on the collapse pressure P_c which leads to a potential relationship between P_c and q^* defined by an exponent factor R. This exponent factor depends linearly on the geometric thickness-to-diameter ratio w/D for inelastic behavior. Therefore the value of R quantifies the effect of the material strain rate dependency with failure pressure for a specific liner geometry. It also remains as future work to evaluate the prediction capability of the TNM model by comparing P_c values obtained from FEM simulations to collapse pressures determined under a controlled experimental setup.

References

[1] E. Engle, HR-370 Pipe rehabilitation with polyethylene pipe liners, 2003.
[2] Canadian Standards Association, CSA Z662-03 Oil and gas pipeline systems, 2003.
[3] K. Goerz, L. Simon, H. Fear, J. Little, Shell Canada Ltd., A Review of Methods for Confirming Integrity of Thermoplastic Liners-Field Experiences, NACE International, Corrosion, March 28–April 1, 2004, New Orleans.
[4] J.F. Mason, J.D. Alkire, Effect of rapid decompression conditions on liner materials 2004. 01 December, 1997, New Orleans, La.
[5] K.E. Szklarz, J.J. Baron, Learnings from thermoplastic liner failures in sour gas pipeline service and replacement liner design and installation, NACE International Corrosion. March 28–April 1, 2004, New Orleans, La.
[6] NACE, RP0304-2004 liners for oilfield pipelines, 2004.
[7] M. Farshad, Plastic Pipe Systems, 1st ed., Elsevier, Great Britain (2006), p. 32–33 134–144.
[8] The Plastics Pipe Institute, Handbook of Polyethylene Pipe. 2nd ed. p. 85–90.
[9] D. Glock, Behavior of liners for rigid pipeline under external water pressure and thermal expansion, Der Stahlbau (1977) 212–217.
[10] S. Jacobsen, Buckling of circular rings and cylindrical tubes under external pressure, Water Power (1974).
[11] K.M. El-Sawy, Inelastic stability of tightly fitted cylindrical liners subjected to external uniform pressure, Int. J. Thin-Walled Struct. (2001) 731–744.
[12] F. Rueda, J.L. Otegui, P.M. Frontini, Numerical tool to model collapse of polymeric liners in pipelines, Eng. Failure Anal. (2011) 24–34.
[13] M.C. Boyce, D.M. Parks, A.S. Argon, Large inelastic deformation of glassy polymers, part, I: rate-dependent constitutive model, Mech. Mater. (1988) 15–33.
[14] E.M. Arruda, M.C. Boyce, A three-dimensional constitutive model for the large stretch behavior of rubber elastic materials, J. Mech. Phys. Solids (1993) 389–412.
[15] E. Arruda, M. Boyce, Effects of strain rate, temperature and thermo-mechanical coupling on the finite strain deformation of glassy polymers, Mech. Mater. (1995) 193–212.
[16] J.S. Bergström, M.C. Boyce, Constitutive modeling of the large strain time-dependent behavior of elastomers, J. Mech. Phys. Solids (1998) 931–954.
[17] J.S. Bergström, M.C. Boyce, Large strain time-dependent behavior of filled elastomers, Mech. Mater. (2000) 620–644.
[18] J.S. Bergström, C.M. Rimnac, S.M. Kurtz, An augmented hybrid constitutive model for simulation of unloading and cyclic loading behavior of conventional and highly crosslinked UHMWPE, Biomaterials (2004) 2171–2178.
[19] J.S. Bergström, J.E. Bischoff, An Advanced Thermo-mechanical Constitutive Model for UHMWPE, Int. J. Struct. Changes Solids (2010) 31–39.
[20] ASTM D638-03, Standard Test Method for Tensile Properties of Plastics, ASTM International, DOI: 10.1520/D0638-03.
[21] A.S.T.M. D0695-02A, Standard Test Method for Compressive Properties of Rigid Plastics, ASTM International. DOI: 10.1520/D0695-02A.
[22] PolyUMod–A Library of Advanced User Materials v. 2.4.2, User's Manual. ©Veryst Engineering LLC, 2013.
[23] J. Bergstrom, Introduction to MCalibration, Software Tutorial, Veryst Engineering LLC, 2013.⟨www.veryst.com⟩.
[24] J.A. Nelder, R. Mead, A simplex method for function minimization, Comput. J. 7 (1965) 308–313.
[25] Abaqus Analysis User´s Manual, 2010, Section 11.5.1, DassaultSystèmes, 2010.
[26] S.R. Frost, A.M. Korsunsky, Y.-S. Wu, A.G. Gibson, 3-D Modeling of liner collapse. In: Conference NACE, 2000.
[27] R.M. Bakeer, M.E. Barber, S.E. Pechon, J.E. Taylor, S. Chunduru, Buckling of HDPE liners under external uniform pressure, J. Mater. Civil Eng. 11 (4) (1999) 353–361.
[28] R.J. Young, P.A. Lovell, Introduction to Polymers, second edition, Chapman & Hall, London, UK (1991), p. 340–344.
[29] N.S.J. Al-Maliky, Strain rate behaviour of thermoplastic polymers, Loughborough University, 1997 (Doctoral Thesis).